

Porous microwells for geometry-selective, large-scale microparticle arrays

Jae Jung Kim^{1†}, Ki Wan Bong^{2,3†}, Eduardo Reátegui^{2,4}, Daniel Irimia^{2*} and Patrick S. Doyle^{1*}

Large-scale microparticle arrays (LSMAs) are key for material science and bioengineering applications. However, previous approaches suffer from trade-offs between scalability, precision, specificity and versatility. Here, we present a porous microwell-based approach to create large-scale microparticle arrays with complex motifs. Microparticles are guided to and pushed into microwells by fluid flow through small open pores at the bottom of the porous well arrays. A scaling theory allows for the rational design of LSMAs to sort and array particles on the basis of their size, shape, or modulus. Sequential particle assembly allows for proximal and nested particle arrangements, as well as particle recollection and pattern transfer. We demonstrate the capabilities of the approach by means of three applications: high-throughput single-cell arrays; microenvironment fabrication for neutrophil chemotaxis; and complex, covert tags by the transfer of an upconversion nanocrystal-laden LSMA.

Large-scale microparticle arrays (LSMAs) have unmatched encoding capacities and rapid decoding capabilities that make them very attractive for a broad range of applications. LSMAs are of utmost interest in biochemical assays^{1–4}, significantly reducing the amount of time and labour. For biomedical applications, spatial positioning of cells in arrays plays an important role in mimicking biological tissues *in vitro* to study cellular behaviour, such as migration⁵ and intercellular communication⁶. The ability to specifically position microparticles enables one to spatially encode chemical or cellular building blocks, resulting in the local control of the microenvironment. For anti-counterfeiting applications, spectrally or graphically coded microparticles are desirable as information carriers because of their high encoding capacity within a small area^{7–9}. Arrangements of multiple microparticles exponentially increase the potential encoding capacity. However, current approaches to position microscale particles in large arrays cannot simultaneously accomplish the requirements of scalability, precision, specificity and versatility that will make LSMAs practical. For example, optical tweezers^{10–12} provide the high resolution of positioning, but can be applied only to small arrays and small dielectric objects with high object-medium refractive index mismatch. Manipulation methods using optoelectronic tweezers¹³ could accomplish large-scale, high-resolution arrangement and sorting, but the technique is unsuitable to generate a heterogeneous pattern containing different types of particle. Magnetic techniques^{14,15} have a limitation in versatility because arranged objects should be doped with magnetic materials. Micro-magnetic robotic coding¹⁶ overcomes this limitation but the technique is unsuitable for large-scale arrangement. Microwells have been used as an assembly template, but are useful only for single-particle arrangement and scaling-up efforts resulted in particle arrangements with some degree of randomness^{1,3,4,17}. Recently it was shown that geometric docking into conformal microwells enables shape-specific positioning, but the technique was limited to a large particle size and significantly long assembly time⁵. Therefore, to achieve the full potential of LSMAs, new

techniques are required to assemble functional microparticles in precise locations that also have high yields and small error rates.

Here, we develop a porous microwell platform to generate LSMAs with high specificity. Microparticles are steered to the microwells via hydrodynamic forces associated with fluid flow through open pores at the bottom of the microwell. Guided microparticles are inserted into congruent microwells, whereas geometrically mismatched particles are removed in a washing step. The forces driving the microparticles to assemble into LSMAs are controllable, have the appropriate magnitude for various microparticles, and are directed towards the wells. By iterative assembly and washing steps, large-scale particle assembly with high yield is demonstrated within 100 s. Shape, size and modulus sorting is achieved with high specificity. We demonstrate that the technique is also compatible with particle recollection and pattern transfer. As a demonstration, we generate a two-dimensional (2D) particle array code for anti-counterfeiting applications, which we then transfer to a precise location on a target substrate. We also generate high-throughput single-cell arrays, and 2D chemokine-releasing particle arrays to study the motility of immune cells in complex-gradient microenvironments.

Design principles for LSMAs

We fabricate porous microwell arrays to generate optimal conditions for particle assembly. We postulate that the ideal driving force for particle assembly should have a direction that points into the assembly template (that is, microwells). Moreover, the force should have a magnitude that is controllable to achieve a high-throughput arrangement without damaging the microparticles during the process. On application of a pressure difference across the porous microwells, the resulting driving force in our platform meets these two criteria: flow streamlines point toward open pores inside the microwells, and the magnitude of the driving force is proportional to the applied pressure difference across the well (Fig. 1b). We fabricated the microwell arrays on top of a porous polyethylene terephthalate (PET) membrane (Fig. 1d) and fine-tuned their

¹Department of Chemical Engineering, Massachusetts Institute of Technology, Cambridge, Massachusetts 02139, USA. ²BioMEMS Resource Center, Massachusetts General Hospital, Harvard Medical School, and Shriners Hospital for Children, Massachusetts 02129, USA. ³Department of Chemical and Biological Engineering, Korea University, 02841, South Korea. ⁴Massachusetts General Hospital Cancer Center, Harvard Medical School, Massachusetts 02129, USA. [†]These authors contributed equally to this work. *e-mail: dirimia@mgh.harvard.edu; pdoyle@mit.edu

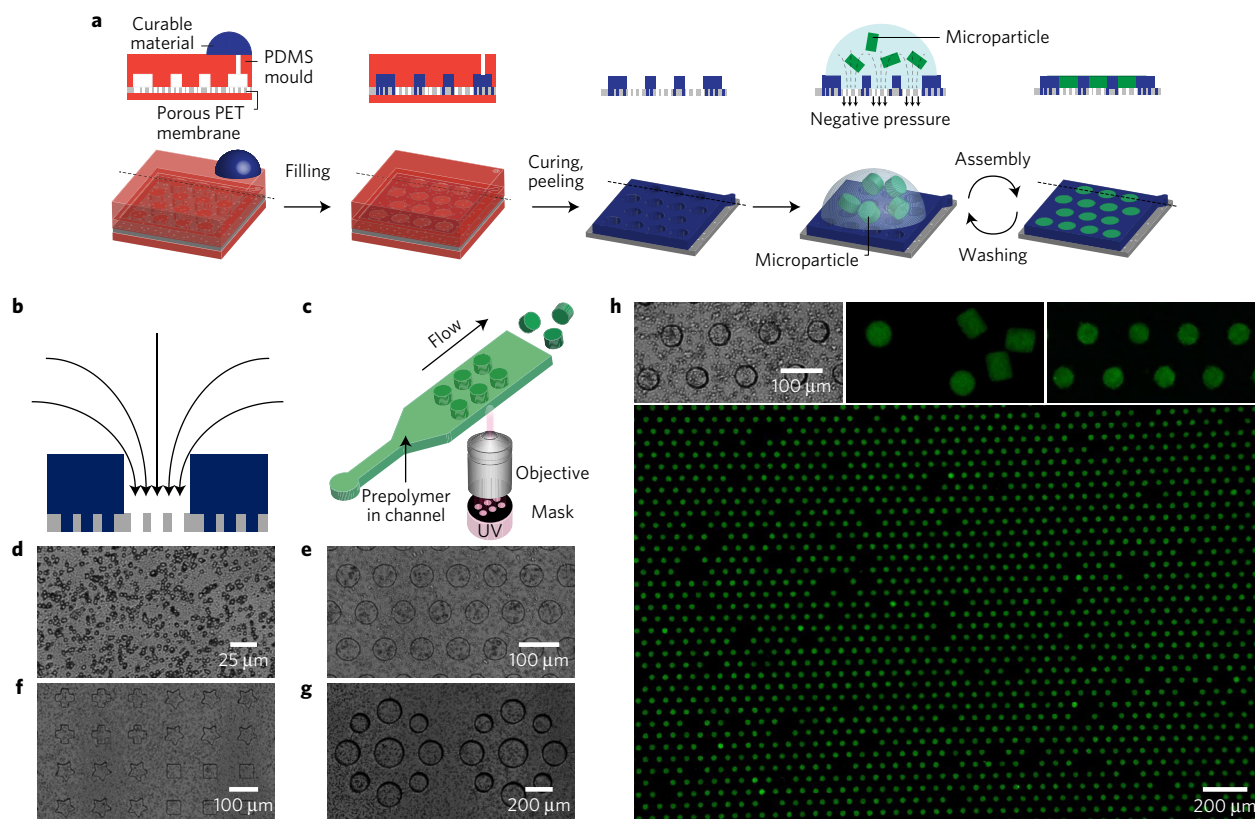


Figure 1 | Porous microwells for microparticle arrays. **a**, Porous microwell fabrication and microparticle assembly. **b**, Direction of negative-pressure-induced driving force of porous microwell arrays. **c**, Synthesis of microparticles by stop flow lithography. **d**, Porous PET membrane (pore diameter: $3\ \mu\text{m}$). **e–g**, Geometry fine-tuned microwell arrays with photocurable NOA (**e,f**) and thermal-curable PDMS (**g**). **h**, Large-scale (3,800), high-throughput microparticle assembly: porous NOA microwell arrays (top left), PEGDA microparticles (top middle), assembled PEGDA microparticle arrays in close (top right) and wide view (bottom).

geometry with the aid of a polydimethylsiloxane (PDMS) mould (Fig. 1a). The mould and the flat PDMS were assembled at the top and bottom of the PET membrane respectively, and a curable material was injected into the mould. Pores that were in contact with the mould were not filled by the curable material. After we cured the microwells, the PDMS mould was peeled away to leave the porous microwell arrays. Both photocurable Norland optical adhesive (NOA; Fig. 1e,f) and thermal-curable PDMS (Fig. 1g) were successfully used to fabricate microwells with distinct shapes, sizes and arrangements (see Supplementary Figs 5 and 6 for porous microwells made by a variety of photo/thermal-curable materials).

Microparticles to be assembled were synthesized by stop flow lithography with a throughput of 10^5 particles h^{-1} (refs 1,2,7,8) (Fig. 1c), and stored in aqueous solution. The particle synthesis throughput can be increased two orders of magnitude by using contact flow lithography¹⁸, which is an advanced form of stop flow lithography. To show the widespread potential of our platform, we synthesized and assembled various microparticles from two very different sets of prepolymer solutions. Soft, biocompatible microparticles, which are widely used in bioassays and microenvironment fabrication, were synthesized from a poly(ethylene glycol) diacrylate (PEGDA) prepolymer solution. More rigid and thermally stable microparticles for anti-counterfeiting applications were made from a mixture of polyurethane acrylate (PUA) and acrylic acid (AA).

Microparticle assembly in microwells

To generate LSMA, a particle suspension was deposited on top of the microwells, and a negative pressure was applied to the bottom of the array. Microparticles were guided to microwells

via fluid flow through the open pores and assembled into shape-matched microwells. Within 10 iterations of assembly and washing, where each cycle takes approximately 10 s, large-scale (3,800) PEGDA microparticle arrays were successfully generated (Fig. 1h, see Supplementary Figs. 7–10 for the largest particle array (15,000) and the smallest assembled particles ($15\ \mu\text{m}$)). The applied pressure deformed the soft PEGDA microparticles to squeeze them into slightly smaller but geometrically conformal microwells. Once pushed inside a microwell, the compressed microparticle will push on the side wall of the microwell, which in turn helps to keep a particle in the well during successive wash and assembly steps. This ability to keep particles retained within a well during successive assembly steps, and the ideal driving force directed into the microwells ensure high assembly yield. In Fig. 1h, $93.7 (\pm 0.8)\%$ of the microwells were filled with particles, and $87.3 (\pm 0.7)\%$ of the initially deposited particles were assembled into microwells.

Physics of the LSMA assembly

Ad hoc choice of microwell dimensions, particle attributes and operating conditions would limit the utility of our approach. For example, it is possible to increase the magnitude of the driving force to increase the assembly speed, but eventually particles will be damaged and result in nonspecific particle assembly—a particle with a square cross-section could be jammed into a non-conformal cylindrical well. Understanding the physics behind the assembly process allows us to tune the driving force and engineer characteristics of the microwells and microparticles to achieve highly specific assembly of complex motifs. Here, we introduce the key dimensionless parameters governing operation of the devices.

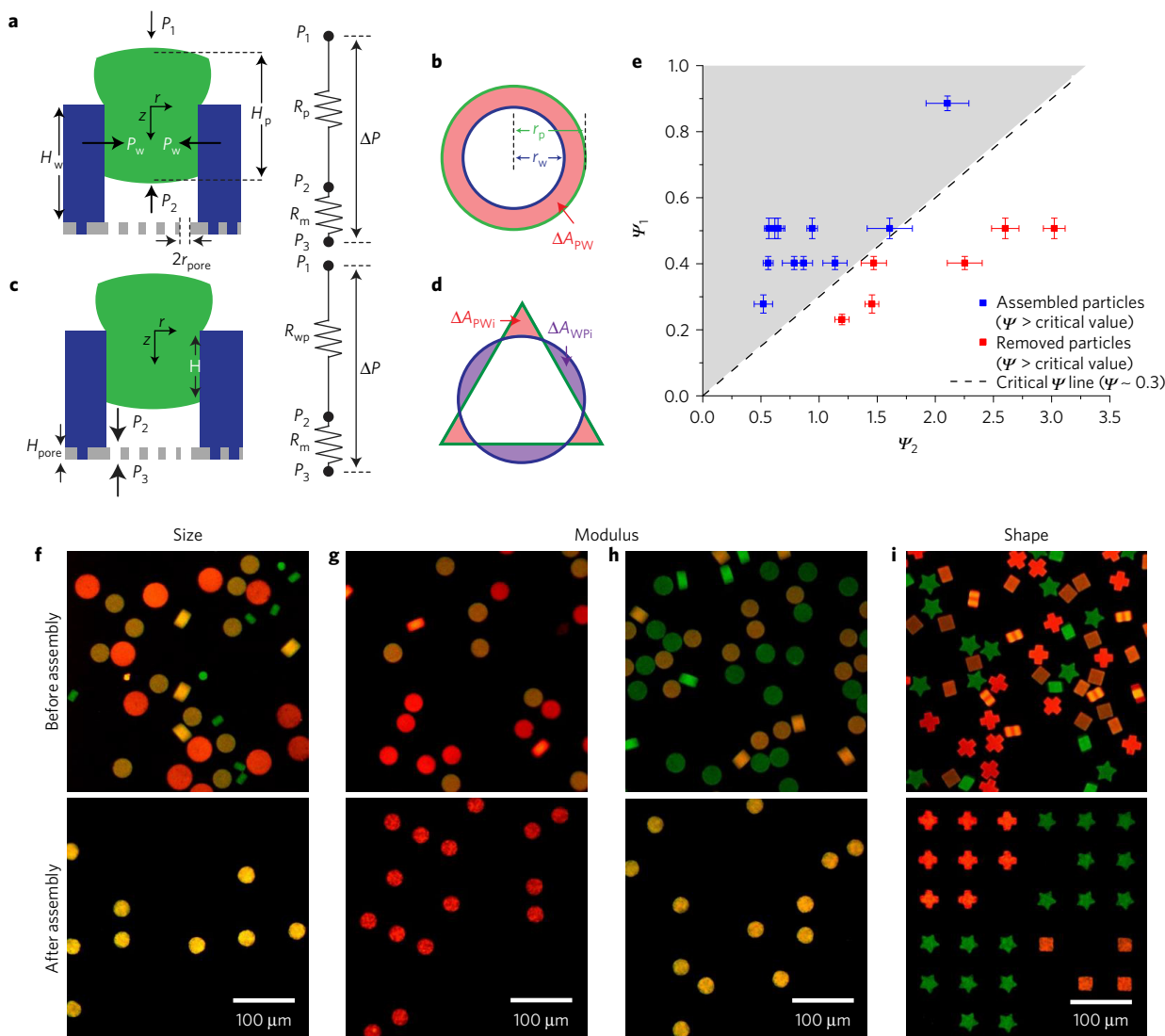


Figure 2 | Scaling analysis and characteristic-specific positioning. **a–d**, Schematics for scaling analysis: shape-matched (**a,b**) and shape-mismatched cases (**c,d**) as side (**a,c**) and top views (**b,d**). Schematics of hydrodynamic resistance of platform are shown next to the side view (**a,c**). **e**, Phase diagram, Ψ_1 as a function of Ψ_2 , for particle assembly in shape-matched cases. PEGDA particles fit into NOA microwells only when Ψ is larger than the critical value (≈ 0.3). **f–i**, Characteristic-specific positioning of particles based on size (**f**), modulus (**g,h**) and shape (**i**). **f**, Diameters of green, yellow and red particles are 30, 60 and 81 μm , respectively. Only yellow particles fit into 54 μm microwells. **g,h**, Moduli of green, yellow and red particles are 240, 140 and 63 kPa. Diameters of particles are 63 μm (**g**) and 59 μm (**h**). Particles with a smaller modulus than the critical value in each case can fit into 54 μm microwells. **i**, Shapes of green, yellow and red particles are star, square and cross respectively while all particles have same modulus and size. Particles fit into only congruent microwells. Specificities of positioning are 96.6 (± 1.8)% (**f**), 97.5 (± 2.2)% (**g**), 95.8 (± 5.3)% (**h**) and 98.8 (± 0.8)% (**i**). Error bars represent standard deviation ($n = 3, 4$).

Consider a soft PEGDA particle that conformally blocks the entrance of a microwell. The force originated from the applied pressure difference (ΔP) is balanced with the wall friction (Fig. 2a). By using the theory behind the interference fit¹⁹ and capillary micromechanics^{20,21}, scaling analysis is conducted to define the dimensionless number Ψ governing particle assembly that is the ratio of the applied pressure difference to the wall friction (see the Supplementary Information for the derivation).

$$\Psi \sim \frac{\Delta P}{\mu E_p} \frac{r_p r_w^2}{H_p \Delta A_{pw}} \quad (1)$$

where ΔP is the applied pressure difference, E_p is the compressive modulus of the particle, r_p is the radius of the particle, r_w is the radius of the microwell, μ is the friction coefficient between the microwell and the particle ($\sim 10^{-3}$ for hydrogel particles²²), H_p is

the height of the microparticle, and $\Delta A_{pw} (= \sum_i \Delta A_{pwi})$ is the area of the particle cross-section that sticks out from the cross-section of the microwell (Fig. 2a–d). We can recognize that Ψ is the ratio of two dimensionless numbers: the combination of the applied pressure difference and materials' properties (Ψ_1); and a purely geometric group (Ψ_2).

$$\Psi_1 \sim \frac{\Delta P}{\mu E_p} \quad (2)$$

$$1/\Psi_2 \sim \frac{r_p r_w^2}{H_p \Delta A_{pw}} \quad (3)$$

Microparticles are assembled into microwells only when the dimensionless parameter Ψ is larger than a critical value, that is, when applied pressure overcomes wall friction. This criterion is

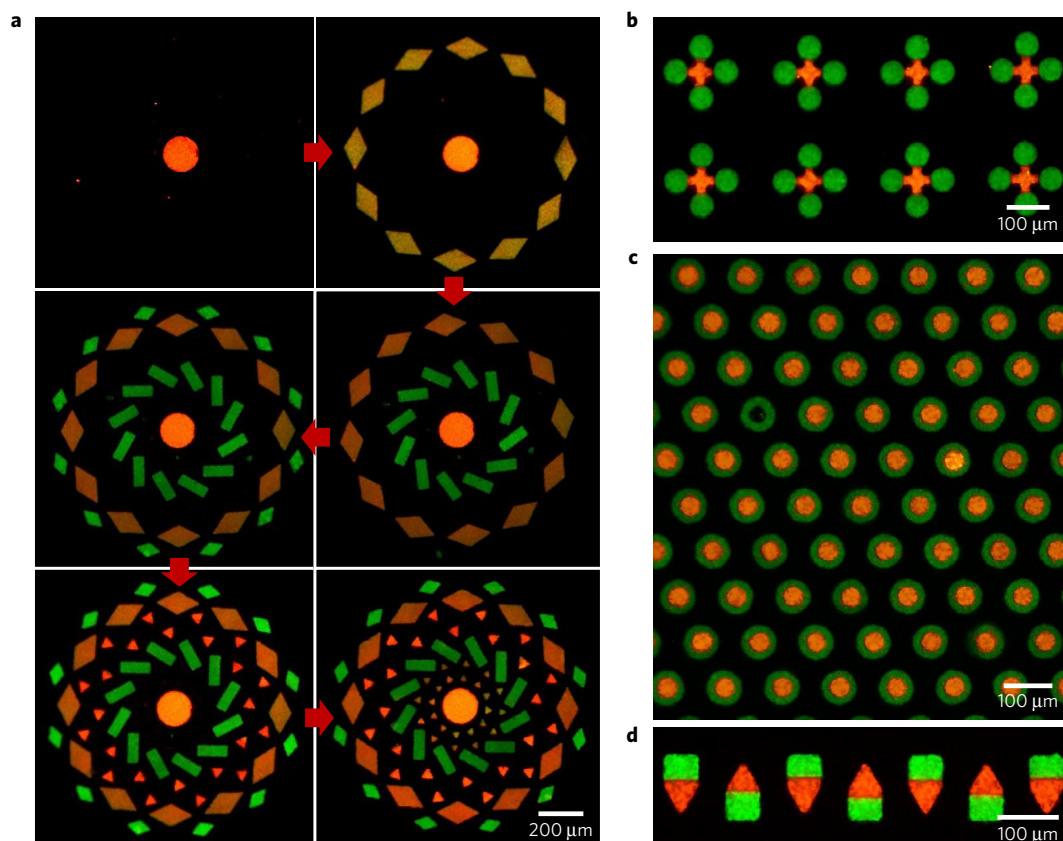


Figure 3 | Advanced assembly techniques. **a**, Sequential assembly for biocompatible, complex microparticle array fabrication. PEGDA particles are assembled in order of size while pre-assembled particles remain in the microwells. **b,c**, Sequential assembly of microparticles at proximal locations. Green particles are assembled before red particle assembly. **d**, Oriented assembly of Janus microparticles. Particles and microwell arrays were made of PEGDA and NOA 81, respectively.

confirmed by plotting Ψ_1 as a function of Ψ_2 , and the critical value of Ψ is found as 0.3 (Fig. 2e). This scaling analysis allows us to specifically position particles on the basis of their characteristics. Size-specific positioning was successfully demonstrated with high specificity (96.6% for Fig. 2f). Specificity is defined as the number of correctly assembled particles per total number of assembled particles. Particles that are slightly larger than microwells were selectively assembled into microwells, whereas too small particles were inserted but then removed in the washing step. As r_p increases, Ψ_2 increases because ΔA_{pw} increases more rapidly than r_p , resulting in Ψ smaller than the critical value; particles with too large r_p cannot fit into microwells. Likewise, particles of the same size but different modulus can be sorted with high specificity (97.5% for Fig. 2g, and 95.8% for Fig. 2h) due to the dependence of Ψ on E_p . Soft particles were successfully sorted from hard particles and positioned in wells (Fig. 2g); as E_p increases, Ψ_1 decreases, resulting in Ψ smaller than the critical value. As r_p decreases, more rigid particles were able to fit into microwells (Fig. 2h; see Supplementary Fig. 16 for the relationship between r_p and E_p).

Even though particles have the same dimension and modulus, they can be specifically positioned depending on another characteristic, shape (Fig. 2i). If the shape of a microparticle is not matched with the microwell shape, the assembly driving force acting on the particles becomes significantly smaller than the shape-matched case—because the hydrodynamic resistance of the membrane (R_m) is much larger than that of the uncovered area (that is, gaps) (R_{wp}) between the microparticle and microwell (Fig. 2c), the pressure difference across the particle becomes much smaller than the pressure difference across the microwell. A dimensionless

number for the shape-mismatched case is (see the Supplementary Information for the derivation)

$$\psi_{\text{mis}} \sim \frac{D_{\text{pore}} H_p A_{\text{pore}}^2}{H_{\text{pore}} \sum \Delta A_{\text{wpi}}^2} \frac{\Delta P}{\mu E_p} \frac{r_p r_w^2}{H_p \Delta A_{\text{pw}}} \sim C \Psi \quad (4)$$

$$C \sim \frac{D_{\text{pore}} H_p A_{\text{pore}}^2}{H_{\text{pore}} \sum \Delta A_{\text{wpi}}^2} \quad (5)$$

where D_{pore} is the number of pores inside a microwell, A_{pore} is the cross-section area of the pore, H_{pore} is the height of the pore, and ΔA_{wpi} is the cross-section area of a microwell not covered by a microparticle (Fig. 2c,d). The ratio of pressure difference across the particle to ΔP is defined as a dimensionless number C , which is also the ratio of particle assembly driving force between shape-matched and mismatched cases. As C is much smaller than 1, high specificity of shape sorting was achieved in Fig. 2i (98.8%, the phase diagram for Fig. 2i is shown in Supplementary Fig. 17).

In a bioassay, the sensitivity for target molecule (for example, microRNA, DNA, protein) detection depends on the porosity and surface area of the particle probe region^{23,24}. Thus, shape-sorted particles with the same gel properties will have the same sensitivities and are useful in multiplexed bioassays.

Encoding capacity of the LSMA is the product of each physical characteristic specifying positioning, size and stiffness, and does not depend on the chemical functionality of particles. To our knowledge, this is the best result to place microparticles at a precise location depending on the largest number of physical characteristics (=3) with the highest specificity and resulting in the highest encoding capacity.

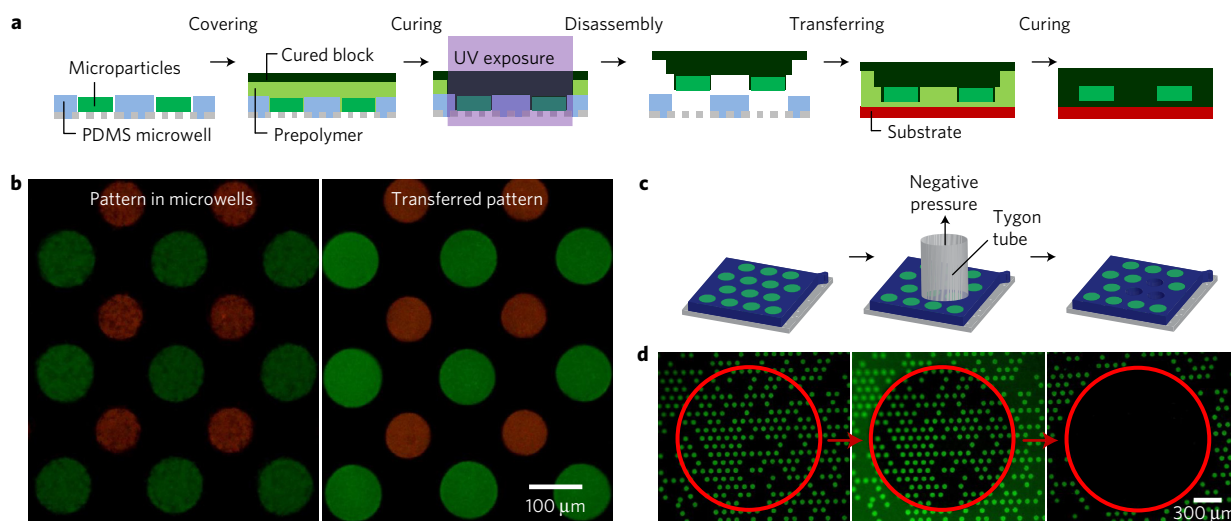


Figure 4 | Post-assembly techniques. **a**, Schematic of pattern transfer with PDMS microwell arrays. **b**, Biocompatible PEGDA microparticle arrays before (left) and after (right) the transfer to the glass slide. **c,d**, Schematic (**c**) and results (**d**) of particle recollection. PEGDA microparticles inside the red circled area (inner diameter of Tygon tube) were selectively recollected from NOA microwells. In the middle image, the inner diameter of the Tygon tube is discerned due to the autofluorescence of the tube.

LSMAs with complex structures

High encoding capacity and persistent positioning of particles in LSMA allowed PEGDA microparticles to be assembled sequentially in order of size to generate the complex motif shown in Fig. 3a. With previous approaches, particles did not maintain their positions during iterative assembly⁵, so it was impossible to assemble microparticles sequentially to generate perfectly filled arrays. Multiple particles can be assembled not only into different microwells, but also at a proximal or nested location inside one microwell. Using sequential assembly, the first set of microparticles was assembled in microwells but did not fully occupy all space in the well, and the second set of microparticles filled the rest of the open space left in a microwell. Particles were located next to each other (Fig. 3b), or inside the hole of another particle (Fig. 3c). These types of arrangement generate the interface of two particles that is critical for the intercellular communication by direct contact⁶. To our knowledge, this is the first demonstration of non-spherical microparticle assembly resulting in direct particle contact via a microwell approach.

Thus far, encoding capacity was generated by positioning microparticles at precise locations depending on their characteristics. However, this post-synthesis processing is not the only way to generate codes. Chemically anisotropic microparticles (for example, Janus or multi-stripped) can be synthesized by co-flowing multiple laminar streams in microfluidic channels during the particle synthesis²⁷. In Fig. 3d, we demonstrate that Janus particles can be arrayed with a specified orientation in the LSMA. Encoding capacity can be exponentially scaled using the combination of the particle's chemical anisotropy (for example, chemically distinct stripes) and particle arrangement.

LSMA transfer techniques

Compared with optoelectronic tweezer¹³ and microfluidic techniques^{25,26}, in our approach the arranged particles are not confined in a closed system. Therefore, particle arrays can be readily repositioned via particle recollection or pattern transfer techniques. Assembled microparticles were recollected by shear stress associated with pressure-driven fluid flow through a Tygon tube (Fig. 4c). Microparticles that were positioned inside the inner diameter of the Tygon tube were selectively recollected (Fig. 4d). After recollection, particles restored to their original size with negligible shrinkage (<2 %).

The pattern transfer technique requires oxygen-permeable PDMS microwell arrays (Fig. 4a). After particle assembly, prepolymer solution was spread on top of the arrays and covered with a pre-cured polymer block. Ultraviolet light (365 nm) was used to cure the prepolymer locally, above the particle arrays to be transferred. While the cured prepolymer chemically bonded with the microparticles and pre-cured block, the prepolymer near the PDMS microwells remained uncured because the oxygen permeability of the PDMS generates an oxygen inhibition layer²⁷. Microparticle patterns were transferred with the pre-cured block while their relative positions were accurately preserved. In one example, biocompatible PEGDA microparticle arrays were successfully transferred to a glass slide (Fig. 4b).

LSMAs for biological applications

The ability to generate large arrays of cells is important for cell-screening applications, when the yield, throughput and ability to repeatedly image the same cells are critical. For example, arranging cells in 2D arrays for the study of cellular processes that progress over time has significant advantages compared with serial approaches, such as flow cytometry²⁸. Cells in a 2D array can be analysed more than once and several cells imaged simultaneously²⁹ for higher yield and to avoid potential differences between the first and last cell analysed that are typical issues for flow cytometry. Here, we tested the performance of LSMA techniques by trapping mammalian glioma cells (U87) in 25- μm -diameter wells, spaced at 25 μm apart. We generated arrays of more than 10,000 cells with high yield. The time required to achieve an acceptable yield for each array was approximately 60 s (Fig. 5a and Supplementary Figs 29 and 30), significantly faster than passive cell settling in microwells, which requires between 5 and 40 min (refs 30,31). Compared with existing technologies^{28–31}, our platform provides a way to arrange cells with high throughput and enables massively parallel imaging.

Guided by chemical gradients, leukocytes display typical migratory responses toward infection and inflammation sites^{32,33}. Multiple cytokines are usually involved, in heterogeneous patterns in tissues³⁴, and distinct patterns of migration are elicited by each cytokine³⁵, resulting in complex leukocyte responses. This complexity is lost in current state of the art *in vitro* assays that probe leukocyte responses to one cytokine at a time, in uniform gradients, and lack the ability to generate 2D heterogeneous chemical gradients^{36–38}. Using our platform's ability to generate complex arrays,

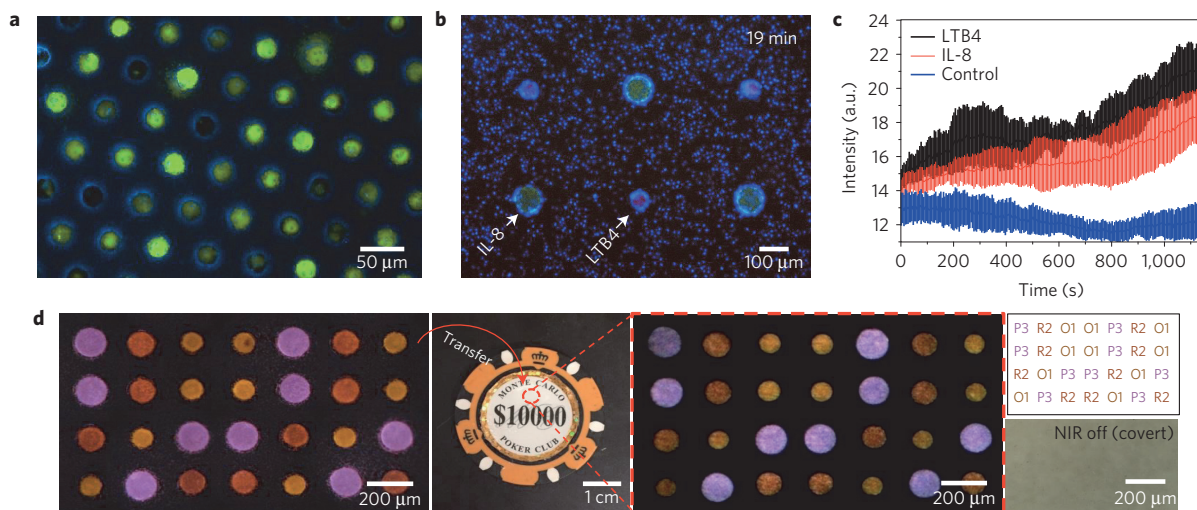


Figure 5 | Application of large-scale microwell arrays. **a**, High-throughput single-cell arrays using a glioma cell line (U87) and porous microwells. Cells that are slightly larger than a microwell are squeezed into the microwells. Cells that are smaller than the microwells remain trapped inside the microwells after the washing step. **b,c**, Larger particles (green), loaded with protein chemoattractant IL-8, and smaller particles (red), loaded with leukotriene chemoattractant LTB4, are arranged in a regular, alternate pattern using LSMA. Human neutrophils (blue) navigate in the heterogeneous microenvironment created by the diffusion of the two chemoattractants from the particles. **b**, Neutrophils accumulate preferentially around the LTB4 source particles after 19 min. **c**, Neutrophil accumulation is quantified by the change in average intensity around source particles over time (blue fluorescence channel). Neutrophil accumulation is slightly faster around LTB4 than IL-8 particles. The control is a region of the array with no particles. Error bars represent standard deviation ($n = 3$). **d**, Anti-counterfeiting demonstration. Sequentially assembled 4×7 code was transferred to a target object (poker chip) and decoded into a text form. From the left, the images show sequentially assembled UCN-laden microparticles, a surface-encoded object (poker chip), transferred particle arrays under NIR exposure, decoded results in a text form (top), and a bright-field image of the encoded area (red circled area on poker chip). In the decoding results, the alphabet character and number represent the colour (Supplementary Table 4) and size of the particles, respectively.

we generated a heterogeneous biochemical microenvironment for the study of neutrophil chemotaxis (Fig. 5b,c). Here, we arranged two distinct chemoattractant-laden microparticles loaded with leukotriene B4 (LTB4) and interleukin-8 (IL-8) in alternate patterns with $300 \mu\text{m}$ spacing. We took advantage of the ability of LSMA techniques to arrange the microparticles quickly before a significant amount of chemoattractant diffuses out of the particles on wetting. We observed the migration patterns of neutrophils in response to the adjacent LTB4 and IL-8 gradients in the array (Fig. 5b). Neutrophils showed migratory responses with a high directional persistence toward LTB4-laden particles and migratory response with no directionality in the vicinity of IL-8 particles (Supplementary Figs 32 and 33). The consequence of the two distinct migration patterns was a larger accumulation of neutrophils around the LTB4-laden particles (Fig. 5c). These results are consistent with previous reports of cell migration in competing gradients of LTB4 and IL-8³⁹. Moreover, they underline the contributions of distinct migration patterns to steering neutrophil populations precisely towards targets in complex microenvironments. These results also underscore the unique characteristics of high throughput, precision, and large-scale manipulation of individual targets, which clearly surpass the abilities of current techniques employing micropipettes⁴⁰ or optically trapped beads³⁶.

LSMAs for anti-counterfeiting applications

To demonstrate the encoding/decoding capacity of LSMAs, we generated a 2D arrangement of upconversion nanocrystal (UCN)-laden PUA/AA microparticles for use in anti-counterfeiting. UCNs, synthesized in large quantity⁴¹, emit the rationally fine-tuned visible light^{7,42} under near-infrared (NIR) exposure via an upconversion process. A covert pattern shows spectrally distinct codes with a single NIR excitation source, resulting in an appealing platform for the security technologies^{7,43}. A direct ink jet printing method has generated a multicoloured, covert pattern, although with a limited precision and resolution⁴³. Soft lithography⁴⁴ (for example,

microcontact printing) requires a manual alignment of multiple components⁴⁵, which is not easily achievable. Compared with those conventional patterning methods, our approach is attractive to anti-counterfeiting application because it generates a high-resolution, multicomponent pattern by using a prealigned microwell array. For 2D particle arrays, encoding capacity scales as $C^S \times S^M$, where C is the number of distinctive colours of the UCNs, S is the number of microparticle sizes, which is used as a characteristic for specific positioning, and M is the number of microwells. For example, by arranging particles with an individual encoding capacity of 27 (3 different size microparticles and 9 distinct UCN colours) into 36 microwells, we exponentially increased the encoding capacity to 10^{20} (Supplementary Fig. 35b)—enough to encode every grain of sand on the Earth ($< 10^{19}$). Not only a 6×6 rectangular pattern, but also other rectangular matrices (Fig. 5d) or even a circular pattern (Supplementary Fig. 35c) can be used. As particles were located at precise locations and in the same optical plane, particle ensembles can be readily decoded (Fig. 5d and Supplementary Fig. 36). Also, this approach avoids potential problems such as tilting, overlapping or touching of particles. The LSMA can be transferred to a target surface (Fig. 5d). Transferred particles were covert without NIR exposure because their refractive index was closely matched with the PUA resin used to transfer and adhere them to the target object. An image of the transferred pattern was taken with an iPhone under NIR exposure and was successfully decoded into a text form within 10 s.

Outlook

Our new LSMA platform enables one to position microparticles at precise locations depending on their physical characteristics with high scalability, precision, specificity and versatility. Assembly in a given microwell is uncoupled from adjacent microwells, leading to a robust, parallelized and scalable process. Our approach is a top-down assembly process wherein the microparticles' locations are predefined by the microfabrication of the microwell template,

ensuring a high precision. Design rules based on a model of the system combined with the ability to fine-tune the properties of the microwells and microparticles enables the resulting high specificity. The hydrodynamic driving force is not limited by particle composition, allowing our assembly method to be applied to a variety of microparticle chemistries.

We expect that the desirable performance of our approach will expand the utility of microparticles and microparticle arrays in many areas. LSMA allows for the generation of increasingly complex and covert codes that can be transferred to a variety of surfaces to expand the utility of particle-based anti-counterfeiting. LSMA of chemokine loaded particles could help replicate the biochemical heterogeneity of tissues at microscale for a variety of biological studies of immune cell responses, development, or tissue engineering. Complex arrangements of cells have great potential for large-scale studies of cell–cell communication and for the monitoring of cellular response over time²⁹. The fast flow-assisted assembly of LSMA will greatly increase the speed and efficiency of existing microwell-based single-cell assays⁴⁶ and potentially expand their applications to include the selective collection of a subpopulation of cells on the basis of physical characteristics⁴⁷. The ability to arrange small objects at proximal locations will pave the way to assemble functional microelectromechanical system components, such as microgears⁴⁸, to tailor acoustic properties of materials⁴⁹ or to develop new bioassays that take advantage of the proximal location of a single cell and particle within a microwell. We envision that this robust LSMA platform will inspire other particle manipulation techniques and find utility in a variety of material science and bioengineering applications.

Methods

Methods and any associated references are available in the [online version of the paper](#).

Received 25 January 2016; accepted 1 August 2016;
published online 5 September 2016

References

- Chung, S. E. *et al.* One-step pipetting and assembly of encoded chemical-laden microparticles for high-throughput multiplexed bioassays. *Nat. Commun.* **5**, 3468 (2014).
- Pregibon, D. C., Toner, M. & Doyle, P. S. Multifunctional encoded particles for high-throughput biomolecule analysis. *Science* **315**, 1393–1396 (2007).
- Walt, D. R. Techview: molecular biology. Bead-based fiber-optic arrays. *Science* **287**, 451–452 (2000).
- Rissin, D. M. *et al.* Single-molecule enzyme-linked immunosorbent assay detects serum proteins at subfemtomolar concentrations. *Nat. Biotechnol.* **28**, 595–599 (2010).
- Eng, G. *et al.* Assembly of complex cell microenvironments using geometrically docked hydrogel shapes. *Proc. Natl Acad. Sci. USA* **110**, 4551–4556 (2013).
- Hui, E. E. & Bhatia, S. N. Micromechanical control of cell–cell interactions. *Proc. Natl Acad. Sci. USA* **104**, 5722–5726 (2007).
- Lee, J. *et al.* Universal process-inert encoding architecture for polymer microparticles. *Nat. Mater.* **13**, 524–529 (2014).
- Han, S. *et al.* Lithographically encoded polymer microtaggant using high-capacity and error-correctable QR code for anti-counterfeiting of drugs. *Adv. Mater.* **24**, 5924–5929 (2012).
- Bae, H. J. *et al.* Biomimetic microfingerprints for anti-counterfeiting strategies. *Adv. Mater.* **27**, 2083–2089 (2015).
- Curtis, J. E., Koss, B. A. & Grier, D. G. Dynamic holographic optical tweezers. *Opt. Commun.* **207**, 169–175 (2002).
- Hoogenboom, J. P., Vossen, D. L. J., Faivre-Moskalenko, C., Dogterom, M. & van Blaaderen, A. Patterning surfaces with colloidal particles using optical tweezers. *Appl. Phys. Lett.* **80**, 4828–4830 (2002).
- Xin, H. B., Xu, R. & Li, B. J. Optical trapping, driving, and arrangement of particles using a tapered fibre probe. *Sci. Rep.-Uk* **2**, 818 (2012).
- Chiou, P. Y., Ohta, A. T. & Wu, M. C. Massively parallel manipulation of single cells and microparticles using optical images. *Nature* **436**, 370–372 (2005).
- Grzybowski, B. A., Stone, H. A. & Whitesides, G. M. Dynamic self-assembly of magnetized, millimetre-sized objects rotating at a liquid–air interface. *Nature* **405**, 1033–1036 (2000).
- Tasoglu, S. *et al.* Guided and magnetic self-assembly of tunable magnetoceptive gels. *Nat. Commun.* **5**, 4702 (2014).
- Tasoglu, S., Diller, E., Guven, S., Sitti, M. & Demirci, U. Untethered micro-robotic coding of three-dimensional material composition. *Nat. Commun.* **5**, 3124 (2014).
- Heo, J. *et al.* Ultra-high-aspect-orthogonal and tunable three dimensional polymeric nanochannel stack array for BioMEMS applications. *Nanoscale* **6**, 9681–9688 (2014).
- Le Goff, G. C., Lee, J., Gupta, A., Hill, W. A. & Doyle, P. S. High-throughput contact flow lithography. *Adv. Sci.* **2**, 1500149 (2015).
- Hamrock, B. J., Jacobson, B. O. & Schmid, S. R. *Fundamentals of Machine Elements* (WCB/McGraw-Hill, 1999).
- Guo, M. Y. & Wyss, H. M. Micromechanics of soft particles. *Macromol. Mater. Eng.* **296**, 223–229 (2011).
- Wyss, H. M., Franke, T., Mele, E. & Weitz, D. A. Capillary micromechanics: measuring the elasticity of microscopic soft objects. *Soft Matter* **6**, 4550–4555 (2010).
- Tominaga, T. *et al.* Effect of substrate adhesion and hydrophobicity on hydrogel friction. *Soft Matter* **4**, 1033–1040 (2008).
- Pregibon, D. C. & Doyle, P. S. Optimization of encoded hydrogel particles for nucleic acid quantification. *Anal. Chem.* **81**, 4873–4881 (2009).
- Choi, N. W. *et al.* Multiplexed detection of mRNA using porosity-tuned hydrogel microparticles. *Anal. Chem.* **84**, 9370–9378 (2012).
- Chung, S. E., Park, W., Shin, S., Lee, S. A. & Kwon, S. Guided and fluidic self-assembly of microstructures using railed microfluidic channels. *Nat. Mater.* **7**, 581–587 (2008).
- Chung, S. E., Jung, Y. & Kwon, S. Three-dimensional fluidic self-assembly by axis translation of two-dimensionally fabricated microcomponents in railed microfluidics. *Small* **7**, 796–803 (2011).
- Dendukuri, D. *et al.* Modeling of oxygen-inhibited free radical photopolymerization in a PDMS microfluidic device. *Macromolecules* **41**, 8547–8556 (2008).
- Cruz, F. C. *et al.* New technologies for examining the role of neuronal ensembles in drug addiction and fear. *Nat. Rev. Neurosci.* **14**, 743–754 (2013).
- Di Carlo, D., Wu, L. Y. & Lee, L. P. Dynamic single cell culture array. *Lab. Chip* **6**, 1445–1449 (2006).
- Rettig, J. R. & Folch, A. Large-scale single-cell trapping and imaging using microwell arrays. *Anal. Chem.* **77**, 5628–5634 (2005).
- Hughes, A. J. *et al.* Single-cell western blotting. *Nat. Methods* **11**, 749–U794 (2014).
- Phillipson, M. & Kubes, P. The neutrophil in vascular inflammation. *Nat. Med.* **17**, 1381–1390 (2011).
- Ridley, A. J. *et al.* Cell migration: Integrating signals from front to back. *Science* **302**, 1704–1709 (2003).
- Sadik, C. D., Kim, N. D. & Luster, A. D. Neutrophils cascading their way to inflammation. *Trends Immunol.* **32**, 452–460 (2011).
- Ng, L. G. *et al.* Visualizing the neutrophil response to sterile tissue injury in mouse dermis reveals a three-phase cascade of events. *J. Invest. Dermatol.* **131**, 2058–2068 (2011).
- Kress, H. *et al.* Cell stimulation with optically manipulated microsources. *Nat. Methods* **6**, 905–909 (2009).
- Boneschansker, L., Yan, J., Wong, E., Briscoe, D. M. & Irimia, D. Microfluidic platform for the quantitative analysis of leukocyte migration signatures. *Nat. Commun.* **5**, 4787 (2014).
- Lin, F. *et al.* Neutrophil migration in opposing chemoattractant gradients using microfluidic chemotaxis devices. *Ann. Biomed. Eng.* **33**, 475–482 (2005).
- Heit, B., Tavener, S., Raharjo, E. & Kubes, P. An intracellular signaling hierarchy determines direction of migration in opposing chemotactic gradients. *J. Cell Biol.* **159**, 91–102 (2002).
- Weiner, O. D. *et al.* Spatial control of actin polymerization during neutrophil chemotaxis. *Nat. Cell Biol.* **1**, 75–81 (1999).
- Wang, F. *et al.* Simultaneous phase and size control of upconversion nanocrystals through lanthanide doping. *Nature* **463**, 1061–1065 (2010).
- Wang, F. & Liu, X. G. Upconversion multicolor fine-tuning: Visible to near-infrared emission from lanthanide-doped NaYF₄ nanoparticles. *J. Am. Chem. Soc.* **130**, 5642–5643 (2008).
- Meruga, J. M. *et al.* Red-green-blue printing using luminescence-upconversion inks. *J. Mater. Chem. C* **2**, 2221–2227 (2014).
- Xia, Y. N. & Whitesides, G. M. Soft lithography. *Annu. Rev. Mater. Sci.* **28**, 153–184 (1998).
- Rogers, J. A., Paul, K. E. & Whitesides, G. M. Quantifying distortions in soft lithography. *J. Vac. Sci. Technol. B* **16**, 88–97 (1998).
- Ogunniyi, A. O., Story, C. M., Papa, E., Guillen, E. & Love, J. C. Screening individual hybridomas by microengraving to discover monoclonal antibodies. *Nat. Protoc.* **4**, 767–782 (2009).

47. Lee, W. C. *et al.* Multivariate biophysical markers predictive of mesenchymal stromal cell multipotency. *Proc. Natl Acad. Sci. USA* **111**, E4409–E4418 (2014).
48. Shepherd, R. F. *et al.* Stop-flow lithography of colloidal, glass, and silicon microcomponents. *Adv. Mater.* **20**, 4734–4739 (2008).
49. Martínez-Sala, R. Sound attenuation by sculpture. *Nature* **378**, 241 (1995).

Acknowledgements

We gratefully acknowledge funding from the National Science Foundation grants CMMI-1120724, a Samsung Scholarship to J.J.K., and National Institutes of Health (GM092804). This work was supported in part by the MRSEC Program of the National Science Foundation under award number DMR-1419807. Microfabrication was performed at BioMEMS Resource Center (EB002503) and MTL, MIT. The modulus measurement was performed in G. McKinley's and A. S. Myerson's laboratories at MIT. We thank B. Hamza and E. J. Lim of the BioMEMS Resource Center for fabrication of Si wafer and insightful discussion, and L. C. Hsiao and H. Burak Eral for the modulus measurement.

Author contributions

J.J.K. and K.W.B. equally contributed to this work. J.J.K. designed the research, conducted the majority of the experiments, conducted a scaling analysis, and interpreted data. K.W.B. conceived the project, obtained preliminary results, and interpreted data. J.J.K. and E.R. designed and demonstrated the biological studies. P.S.D. and D.I. designed the research, supervised the study, and interpreted data. J.J.K., P.S.D. and D.I. wrote the manuscript, and all authors commented on the manuscript.

Additional information

Supplementary information is available in the [online version of the paper](#). Reprints and permissions information is available online at www.nature.com/reprints. Correspondence and requests for materials should be addressed to D.I. or P.S.D.

Competing financial interests

Two provisional US patent applications were filed on 1 November 2013 and 17 August 2016, respectively.

Methods

Porous microwell fabrication. Porous microwell arrays are fabricated with a PDMS (Sylgard 184, Dow Corning) mould on top of a porous PET membrane (Millipore, diameter of pore: 3 μm) (Supplementary Figs 1 and 2). To prepare the mould, PDMS is mixed with curing agents in a 10:1 ratio and cured on a SU-8 (Microchem) master prepared by standard photo-lithography procedures. For PDMS microwell fabrication, the PDMS mould is plasma-treated and functionalized with trichloro(1H,1H,2H,2H-perfluorooctyl)silane (Sigma Aldrich) to ensure the detachment of PDMS microwell arrays from the PDMS mould. The PDMS mould and flat PDMS are placed at the top and bottom of the PET membrane. Curable materials (for example, NOA 81, PDMS) are placed on top of the inlet of mould. The entire device is placed inside a vacuum desiccator. As vacuum is applied, air trapped in the mould is removed, and curable materials are injected to the mould by the pressure difference. After photo (365 nm light) or thermal (65 °C) curing, the PDMS mould and flat PDMS are removed from the porous microwell arrays. For the anti-counterfeiting demonstration, PDMS microwell arrays were plasma-treated, and functionalized with fluorinated silane to increase the hydrophilicity difference between microwells and microparticles, eliminating any undesired adhesion.

Particle assembly. Microparticle solution is dispensed on top of the porous microwell array. Negative pressure is applied at the bottom of porous microwell arrays to generate the driving force for particle assembly. A Kimwipe (Kimberly-Clark) is placed under the NOA microwell arrays to generate the negative pressure due to the capillary wetting (Supplementary Fig. 2i). For PDMS microwells, vacuum suction is used to generate negative pressure (Supplementary Fig. 2k). After particle assembly, redundant particles were washed out by water flow using a squeeze bottle (Supplementary Fig. 2j). Particle assembly and washing steps are repeated to ensure a high yield.

Microparticle synthesis. Microparticles are synthesized in a microfluidic channel via stop flow lithography^{1,2,7,8}. The top part of the PDMS channel (mixed in 10:1

ratio) is cured on SU-8 master overnight at 65 °C, and then placed on the glass slide that is covered by half-cured PDMS (mixed in 10:1 ratio, cured for 20 min at 65 °C). The assembled device is fully cured overnight at 65 °C. The prepolymer solution is flowed through the channel by compressed air, stopped, and exposed by ultraviolet light (365 nm). Ultraviolet light is patterned by a transparency mask (Fineline) designed in AUTOCAD. 2D extruded-shape microparticles are synthesized by photo-crosslinking. Three steps—flow, stop, exposure—are repeated to synthesize the microparticles in a semi-continuous manner. Flushed microparticles are centrifuged and resuspended several times, and then stored in 1 \times TET solution (1 \times Tris-EDTA buffer with 0.05% (v/v) Tween-20).

Particle recollection. Two Tygon tubes are connected to the recollection reservoir. One is connected to a vacuum line, and the other one is used as a recollection tube. Particle arrays are submerged in 1 \times TET solution, and the recollection tube is placed on top of the targeted area using an *xyz* stage. The recollection tube is brought into contact with the array, and vacuum is applied to generate the pressure difference. After a few seconds, the recollection tube is slightly displaced upward to make a gap between the tube and array. The 1 \times TET solution is aspirated through this gap and particles are recollected due to the shear stress associated with the fluid flow.

Pattern transfer. PDMS microwell arrays are desired for pattern transfer due to the lubricating layer provided by oxygen inhibition near the PDMS²⁷. Prepolymer solution is dispensed on assembled particle arrays, and pre-cured polymer block is then placed on top. Ultraviolet light (365 nm) exposes to the targeted area from the bottom. In this exposure step, the oxygen permeability of the PDMS ensures that the prepolymer solution does not stick to the PDMS microwell arrays whereas particles and the pre-cured block are covalently connected by cured prepolymer solution. After UV exposure, uncured prepolymer solution is washed out, and pre-cured block is transferred with attached particle arrays. Fluorinated PDMS microwells were plasma-treated to enhance the spreading of the prepolymer solution.